Food Chemistry: X 23 (2024) 101758

Contents lists available at ScienceDirect

Food Chemistry: X

journal homepage: www.sciencedirect.com/journal/food-chemistry-x

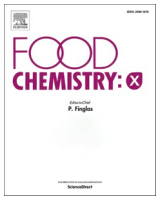

The impact of visible light component bands on polyphenols from red grape seed extract powder encapsulated in alginate–whey protein matrix

A. Mihaly Cozmuta [a,*], A. Peter [a], C. Nicula [a], A. Jastrzębska [b], M. Jakubczak [b], M.A.K. Purbayanto [b], A. Bunea [c], F. Bora [d,e], A. Uivarasan [a], Z. Szakács [a], L. Mihaly Cozmuta [a]

[a] Technical University of Cluj Napoca, North University Center of Baia Mare, Victoriei Str. 76, Baia Mare, Romania
[b] Warsaw University of Technology, Faculty of Mechatronics, 8 Andrzeja Boboli Street, 02-525 Warsaw, Poland
[c] Biochemistry Department, Faculty of Animal Science and Biotechnology, University of Agricultural Sciences and Veterinary Medicine Cluj-Napoca, 3-5 Mănăștur Street, 400372 Cluj-Napoca, Romania
[d] Viticulture and Oenology Department, Advanced Horticultural Research Institute of Transylvania, Faculty of Horticulture and Business in Rural Development, University of Agricultural Sciences and Veterinary Medicine Cluj-Napoca, 3-5 Mănăștur Street, 400372 Cluj-Napoca, Romania
[e] Laboratory of Chromatography, Advanced Horticultural Research Institute of Transylvania, Faculty of Horticulture and Business for Rural Development, University of Agricultural Sciences and Veterinary Medicine, 400372 Cluj-Napoca, Romania

ARTICLE INFO

Keywords:
Grape seed extract encapsulation
Visible light component bands
Color analysis
Reflectance spectra deconvolution

ABSTRACT

Beads made of sodium alginate, whey protein concentrate, and red grape seed extract powder were exposed to white light and its red-orange, yellow-green-cyan, and cyan-blue-violet bands. The chemical analysis showed that encapsulation in the alginate–whey protein matrix protected polyphenols, flavonoids and cyanidin-3-*O*-glucoside when exposed to red-orange light. The reflectance spectra acquired from grape seed extract powder and grape seed extract beads were deconvoluted and anthocyanins-based moieties which contribute to the expression of bathochromic or hypsochromic effects were identified. The evolution of the peak areas assigned to the colored compounds confirms that the most intense polyphenol degradation occurred in grape seed extract powder and grape seed extract beads exposed to cyan-blue-violet light, as shown by the chemical analysis. The results of the study are important in choosing the light band from the visible spectrum which can be used to process food enriched with grape seed extract with minimal polyphenol degradation.

1. Introduction

Technologies based on visible light and its component colors have diverse and effective applications in the food industry, supporting a more sustainable and less wasteful food production chain (Hinds, Bhavya, O'Donnell, & Tiwari, 2022). Visible (white) light combines *electromagnetic radiation of different wavelengths and can be obtained by* mixing red, blue, and green light. Orange, yellow, cyan, and violet light can also be added to reproduce a wider range of hues. *Its application in horticulture, agriculture, and food production can overcome the poor spatio-temporal distribution of sunlight in some regions (*D'Souza, Yuk, Khoo, & Zhou, 2015). In lamb's lettuce, a delay in senescence was observed by increasing the a/b chlorophyll ratio (Braidot et al., 2014), while an increase in the concentrations of total chlorophyll, vitamin C, and total phenolic contents was observed under white light compared to dark storage (Lee, Ha, Oh, & Cho, 2014). Individual components of white light have also been reported to be useful for the food industry. Experimental data have suggested that *blue light* is an effective bactericidal agent against pathogenic and spoilage-causing bacteria in dairy and liquid *foods, meat and seafood products, food packaging, and work surfaces* (Hadi, Wu, & Brightwell, 2020). *The work of* Yeh, Yeh, Shih, Byadgi, and Chih Cheng (2014) *has shown that b*lue light promotes the growth of carotenoids in some species of algae. Red light has been reported to delay the senescence of vegetables and the loss of postharvest nutritional content (Ma et al., 2014). Green light has been shown to prevent discoloration of potatoes caused by increasing solanine and chlorophyll

Abbreviations: CE, catechin equivalents; GAE, gallic acid equivalents; GSEP, red grape seeds extract powder; GSEB, red grape seeds extract beads; R, B, G, red, blue, and green coordinates of RBG color system; TFC, total flavonoids content; TPC, total polyphenols content; C3G, cyanidin-3-O-glucoside; WPC, whey protein concentrate.

* Corresponding author.
E-mail address: ancamihalycozmuta@gmail.com (A. Mihaly Cozmuta).

https://doi.org/10.1016/j.fochx.2024.101758
Received 4 July 2024; Received in revised form 15 August 2024; Accepted 20 August 2024
Available online 22 August 2024

concentration and improve the anthocyanin content of unripe strawberries (Kim et al., 2011).

Grape seeds, by-products of the wine industry, are rich sources of bioactive compounds, such as fiber, oil, proteins, polyphenols, minerals, and salts (Kim, Jeong et al., 2006). Processing grape seeds or solid residues from the wine-making process produces grape seed extract, a heterogeneous mixture which contains >95 % polyphenols such as phenolic acids (gallic acid, *p*-coumaric and *trans*-ferulic acid, tartaric acid, protocatechuic acid, malic acid), and proanthocyanidins (accounting at least 74–78 %) in the form of monomeric phenolic compounds ((+)-catechin and (−) -epicatechin, epicatechin-3-*O*-gallate, flavan-3-ols), and in dimeric, trimeric and tetrameric procyanidin forms (Dabetic, Todorovic, Malenovic, Sobajic, & Markovic, 2022; Gómez-Mejía, Vicente-Zurdo, Rosales-Conrado, León-González, & Madrid, 2022; Perumalla & Hettiarachchy, 2011; Rózek, Achaerandio, Gűel, López, & Ferrando, 2009). Due to their high polyphenols content with phytopharmaceutical properties such as (+)-catechin and (−) -epicatechin, epicatechin-3-*O*-gallate, grape seeds have numerous beneficial effects, including free radical scavenging, antioxidant properties, inhibition of the enzymes that catalyze histamine release responsible for inflammations and allergies, inhibition of low-density lipoprotein oxidation and platelet aggregation (Amico, Chillemi, Mangiafico, Spatafora, & Tringali, 2008; Kim et al., 2006; Rózek et al., 2009). Due to these positive properties, grape seed extract is highly recommended for developing functional foods and dietary supplements. Meat and meat products (Reddy et al., 2013; Ribas-Agusti et al., 2014), potato chips (Sáyago-Ayerdi, Brenes, & Goñi, 2009), and bread (Peng et al., 2010) enriched with grape seed extract have higher shelf life, antioxidant properties, and lipid stability than non-fortified related products. The main challenge in fortifying food with grape seed extract is related to the high sensitivity of polyphenols to the thermal or non-thermal processes that fortified foods are exposed to during production, storage, and processing. Under the action of light, temperature, oxygen, enzymes or pH dimerization, oxidation, hydroxylation, or nucleophilic attack cleavage of polyphenols can occur and result in the loss of their antioxidant activity. The study of Kosović, Topiař, Cuřínová, and Sajfrtová (2020) shows that the concentrations of trans-resveratrol and trans-ε-viniferin obtained from *Vitis vinifera* L. decreased until almost complete decomposition when stored for 14 days at daylight. Quercetin, rutin, peonidin, pelargonidin, p-coumaric, ellagic, and p-hydroxybenzoic acids were found to be the least stable phenolics when exposed to sunlight (Mrázková, Sumczynski, & Orsavová, 2023).

Efforts have been made to improve the resistance of polyphenols to such processes, encapsulation has provided a viable alternative. Sodium alginate mixed with whey protein concentrate, maltodextrins, gum Arabic, cellulose derivatives, chitosan or chitosan–carvacrol to reduce porosity and strengthen the matrix, has been used to encapsulate grape seed extract (Pedrali, Barbarito, & Lavelli, 2020; Yadav, Bajaj, Mandal, & Mann, 2019). Sheng et al. (2021) showed that grape seed proanthocyanidin extract encapsulated in sodium alginate-methyl cellulose and sodium alginate-hydroxypropyl methylcellulose stored for 28 days at 25 °C in natural light resulted in a retention rate higher than 80 %, while retention rate in non-encapsulated sample significantly decreased after 21 days of storage. Encapsulation in chitosan and maltodextrin of anthocyanins from black glutinous rice increased their stability under light exposure for 15 days by 1.47-fold and 1.64-fold compared with non-encapsulated anthocyanins (Vichit, Saewan, & Thitipromote, 2012). Other studies (Chi et al., 2019; Mahdavi, Jafari, Assadpour, & Ghorbani, 2016; Ouyang et al., 2020) also proved the improvement in the light stability and increased half-life of cyanidin-3-*O*-glucoside (C3G) encapsulated in casein, maltodextrin and gum Arabic or nanoliposomal carriers compared to the non-encapsulated C3G.

To the best of our knowledge, there are no studies examining the impact of visible light component bands on the encapsulated polyphenols. From this perspective, the aim of this work is to encapsulate the red grape seed extract in a matrix of alginate–whey protein concentrate and compare the stability of the extract and beads under exposure to white light and its red-orange, yellow-green-cyan, and cyan-blue-violet components.

Considering that the stability of polyphenols is an important factor in producing of food with high nutritional value and antioxidant activity, this study provides valuable insights into the influence of visible light and its component bands on grape seed extract powder and alginate–-whey protein–grape seed extract beads. Thus, a specific light band from the visible spectrum can be chosen to process food enriched with grape seed extract with minimal polyphenol degradation to obtain food with high health beneficial effects.

2. Materials and methods

2.1. Reagents

Sodium alginate (viscosity of 25.7 cps at 25 °C, mannuronic/guluronic ratio of 35/65-data supplied by the manufacturer) was provided by Sigma-Aldrich (USA), whey protein concentrate (70 %) by Gymbeam (Germany), and red grape seed extract powder by Bulk™ Company (England). Analytical grade Folin-Ciocalteu reagent, calcium chloride, sodium carbonate, hydrochloric acid, methanol, ethanol, aluminum chloride, sodium nitrite, sodium hydroxide, ethyl acetate, formic acid, acetonitrile were purchased from Sigma-Aldrich (USA). Standards catechin, gallic acid and cyanidin HPLC grade were purchased from Sigma Aldrich (Saint Louis, MO, USA).

2.2. Encapsulation of red grape seed extract powder

Alginate–whey protein concentrate–red grape seed extract powder beads (GSEB) were prepared using the external ionic gelation method. Alginate-whey-extract solution was extruded as droplets into a gelling bath containing Ca^{2+} which binds the guluronate blocks of the alginate chains forming an "egg-box" structure (Leong et al., 2016). Of the five possible gelling methods namely external, internal, inverse, interfacial, and multi-step interrupted gelation, the external cross-linking method was selected for this study. It requires simple equipment and results in smoother surface, with greater matrix strength and higher encapsulation efficiencies as compared with internal cross-linking method (Chan, Lee, & Heng, 2006).

Different ratios of sodium alginate (SA) and whey protein concentrate (WPC) were first homogenized at 25 °C in 100 mL of ultrapure water (Thermo Fisher Scientific Barnstead™, USA) with stirring to develop the alginate–whey protein binary matrices (Table 1). After 1 h, the red grape seed extract powder (GSEP) was added in different ratios (Table 1) while stirring was continued for another 3 h. A peristaltic pump (PM05 AES Laboratoire, France) delivered the final solution at 65 rpm, followed by extrusion through a capillary tube (diameter 0.5 mm) into a bath containing 500 mL of 0.5 mol/L $CaCl_2$. The resulting beads were kept in the bath for 30 min to achieve gelation, filtered, rinsed with ultrapure water, and dried at 25 °C until they reached a constant weight. Control beads without red grape seed extract powder were also prepared to quantify the contribution of the raw materials to the beads.

All procedures for beads preparation and samples analysis were conducted in the dark at 25 °C to avoid degrading the polyphenols. Samples transportation for further analysis was done in a dark cool box at 4 °C, in the shortest possible time.

2.3. Encapsulation efficiency and selection of the beads

The total polyphenol concentration in GSEB, control beads, and GSEP were determined according to the procedures described in Section 2.6. The encapsulation efficiency was calculated according to the following equation:

$$EE\ (\%) = P_B \times 100/P_P \quad (1)$$

Table 1
Bead compositions and encapsulation parameters.

Composition (w:w:w:v)	Total polyphenols content in the dried sample, mg GA/g sample	Encapsulation efficiency, EE%	The gravimetric yield of the encapsulation process, g
Red grape seed extract powder	72.35	–	–
Alginate:Whey proteins: Extract:Water 1:1:0:100 (control beads)	–	–	–
Alginate:Whey proteins: Extract:Water 1:0:1:100	9.79 ± 0.41^{d}	75.19 ± 2.37^{b}	5.56 ± 0.24^{c}
Alginate:Whey protein: Extract:Water 1:1:1:100	9.64 ± 0.39^{d}	86.43 ± 1.91^{a}	6.48 ± 0.27^{b}
Alginate:Whey proteins: Extract:Water 1:1:2:100	8.47 ± 0.20^{e}	86.19 ± 3.59^{a}	7.36 ± 0.17^{a}
Alginate:Whey protein: Extract:Water 1:2:1:100	13.21 ± 0.66^{b}	88.64 ± 1.98^{a}	4.85 ± 0.41^{cde}
Alginate:Whey proteins: Extract:Water 2:1:1:100	11.93 ± 0.49^{c}	87.29 ± 2.70^{a}	5.29 ± 0.22^{c}
Alginate:Whey proteins: Extract:Water 1:2:2:100	15.60 ± 0.32^{a}	88.08 ± 2.43^{a}	4.09 ± 0.36^{e}
Alginate:Whey proteins: Extract:Water 2:1:2:100	14.89 ± 0.55^{a}	87.70 ± 2.05^{a}	4.26 ± 0.24^{de}
Alginate:Whey proteins: Extract:Water 2.2:1:100	12.53 ± 0.27^{bc}	86.55 ± 2.61^{a}	4.99 ± 0.16^{cd}

Results are expressed as average ± standard deviation ($n = 3$). In each column, mean values marked with different superscript letters are significantly different ($p < 0.05$);
Extract – red grape seed extract powder.

where EE is the encapsulation efficiency of the red grape seed extract powder, P_B is the total polyphenol amount in the dried beads, mg GAE and P_P is the total polyphenol amount in the red grape seed extract powder used to prepare the beads, mg GAE.

The beads with the highest encapsulation efficiency parameters were selected for further investigation.

2.4. Treatments of GSEP and selected GSEB

Four treatments (white light with a wavelength in the range 400–725 nm, red-orange band in the range 600–725 nm, yellow-green-cyan band in the range 475–600 nm, and cyan-blue-violet band in the range 400–550 nm) were applied to the extract powder and the beads. The sample exposure time was calculated so that the irradiated energy in each color band was as close as possible to the energy in the same band when white light irradiation was used. Periodically, the samples were collected and analyzed. The temperatures of the samples during and at the end of exposure never exceed 30 °C. A DLP projector was used to produce the light for the visible light exposure experiments. This DLP projector uses a five-color wheel filter (white-blue-red-yellow-green) for color reproduction and a 200 W Osram TLPLV6 metal-halide lamp assembly with an inherent strong IR/UV-cut filter. To produce the desired illumination, primary white/red/green/blue standard monitor test patterns were displayed at the native resolution and refresh rate of the projector. In this experimental setup, the projector was used as the secondary display of a laptop. A ground-glass light homogenizer and supplementary color glass filters further enhanced the spatial homogeneity and spectral-band distribution definitions of the DLP illuminant; specifically, a Hama HTMC Red R8 (25 A) high-pass filter in combination with the red color test pattern, a Hoya HMC Green X1 band-pass filter with the green color test pattern, and a LZOS Blue 1.4× low-pass filter with the blue color test pattern. The white light experiments were run first. The relative intensity spectral distribution series at the sample plane was recorded with a modular spectrometer connected to the laptop running the AvaSoft 8 spectroscopy software on its primary integrated display. For every white/colored light experiment, at least 150 relative spectral intensity measurement batches, mediated over 100 spectra, were registered at the beginning, middle, and end of each experiment. Each spectrum was measured over 1.05 μs so that the obtained values were sufficiently well separated from black noise, and sensor signal-clipping was avoided. In illumination experiments, keeping this measurement time constant also ensured comparable noise behavior. Strong light filtering for the red/green/blue illumination experiments heavily reduced the light intensity relative to the white illuminant due to the color reproduction principle of the DLP, which employs a digital mirror device and the above-mentioned internal color filters, complemented by our external filtering. More details about the production of the light for the visible light exposure experiments are presented in the Supplementary Material (SM).

All light illumination experiments were conducted in an air-conditioned room at 25 °C, with the air-conditioning turned on at least 24 h before each experiment's start to achieve the desired environmental conditions, without any significant air flux over the experimental setup. The relative humidity fluctuated between 50 and 60 %. After irradiation time ended, each sample was left in the dark in the experimental irradiation chamber, in controlled stable environment, to equate the maximum irradiation time of 12 h for the yellow-green-cyan light. Unexposed samples were also maintained in the same conditions.

2.5. Morphology and microstructure of GSEB

Digital photographs of GSEP and GSEB were taken with a Bresser LCD micro 5MP microscope (Bresser GmbH, Germany). The changes on the surface and in the core of the beads exposed to light treatments were visualized using scanning electron microscopy (SEM; S-3500 N, Hitachi, Japan). To ensure the conductivity of the beads, they were placed on a conductive carbon tape and sputtered with a conductive gold nanoparticle layer before the SEM images were acquired. At least 100 beads of each type were used to measure the shape parameters with ImageJ (National Institutes of Health and Laboratory for Optical and Computational Instrumentation LOCI, University of Wisconsin). To describe the shape of the beads, the area, equivalent diameter, Feret's diameters, perimeter, and sphericity factor were calculated according to the equations presented in the Supplementary Material (SM).

2.6. Total polyphenol content

The total polyphenol content of the samples was determined using the method of Ivanova et al. (2010). An accurately weighed 0.3 g sample of powder and beads was mixed with 20 mL of a 69/30/1 (*v*/v/v) ethanol/water/HCl mixture for 24 h in the darkness at 25 °C with stirring. After filtration conducted through a blue-ribbon filter paper using a Buchner funnel with vacuum suction, 1 mL of extract solution was mixed with 3 mL of Folin–Ciocalteu reagent, 5 mL of distilled water, and 3 mL of 7.5 % (*w/v*) sodium carbonate (Wu et al., 2020). The mixture was kept in the dark at 25 °C for 1 h, and the absorbance was measured at 765 nm

using a Lambda 35 spectrophotometer. Gallic acid was used to standardize the phenolic content. The results are expressed as gallic acid equivalents in 1 g of dry sample for GSEP (mg GAE/g powder) and as gallic acid equivalents in 4.85 g of dry beads for GSEB (mg GAE/4.85 g beads).

2.7. Total flavonoid content

Because they comprise the greatest fraction of the grape seed extract, the total flavonoid contents of GSEP and GSEB were analyzed according to the method described by Ivanova et al. (2010) adapted to our study. A volume of 1 mL of total polyphenol extract solution was mixed with 4 mL of distilled water and 0.3 mL of 0.5 g/L $NaNO_2$ solution. Volumes of 0.3 mL of 0.1 g/L of $AlCl_3$ and 2 mL of 1 M NaOH solutions were added after 5 and 6 min, respectively. Distilled water was added to bring the total volume to 10 mL, and after homogenization, the absorbance of the final solution was measured at 510 nm relative to the water-based blank (Lambda 35 spectrophotometer, Perkin Elmer, USA). Catechin was used to standardize the flavonoid content. The results are expressed as catechin acid equivalents in 1 g of dry sample for GSEP (mg CE/g powder) and in 4.85 g of dry sample for GSEB (mg CE/4.85 g beads).

2.8. Quantification of cyanidin 3-O-glucoside

The influence of light on the concentration of cyanidin 3-*O*-glucoside, the main anthocyanin found in red grape seeds, was also quantified in powder and beads, considering the maximum exposure time (Table 3). The anthocyanins were extracted from samples using the method described by Nile, Kim, and Keum (2015) adapted to this study. The sample (0.3 g) was extracted using 30 mL of acidified methanol (0.3 % HCl) in triplicate under continuous stirring (Miccra D-9 KT Digitronic, Bergheim, Germany). The three extracts were combined and filtered through several layers of cotton and concentrated under vacuum at 35 °C until the methanol was completely removed. Ethyl acetate was used to separate the anthocyanin group from less polar compounds. The resulting extract was diluted to 5 mL with distilled water, filtered through a 0.45-µm membrane filter (MF-Millipore™, Merck-Millipore, Germany), and analyzed using an HPLC-DAD-ESI-MS system (High-Performance Liquid Chromatography–Diode Array Detection–Electro-Spray Ionization Mass Spectrometry) consisting of an Agilent 1200 HPLC with a UV–vis detector (DAD) coupled to a mass detector (MS) with a single quadrupole Agilent 6110 (Agilent Technologies, Santa Clara, CA, USA).

Cyanidin was quantified using a Shimadzu instrument (Japan) equipped with a binary LC-20 AT (Prominence) feed pump, a DGU-20 A3 (Prominence) degasser, an SPM-M20 photodiode detector, a Luna Phenomenex C-18 (5 µm, 25 cm × 4.6 mm) column, and a UV-VIS detector. Two mobile phases were used: mobile phase A consisted of 4.5 % formic acid in bidistilled water, while solvent B was acetonitrile. The chromatographic gradient was as follows: 9 min of 10 % solvent B, 17 min of solvent B from 10 % to 12 %, 30 min of solvent B from 12 % to 25 %, and 90 % solvent B ranging from 30 min to 50 min. A volume of 20 µL of sample was injected into the column at a flow rate of 0.8 mL/min at 35 °C. The cyanidin was quantified at 520 nm using a calibration curve ($r^2 > 0.998$) based on a cyanidin standard in the concentration range of 2.5–500 µg/mL.

2.9. Color analysis

Color measurements were performed on untreated and treated samples after exposure to white light and its red-orange, yellow-green-cyan, and cyan-blue-violet illuminant component bands using a YL 4560-3nh non-contact benchtop spectrophotometer (Shenzhen Threenh Technology Co., Ltd., China) and expressed in RGB (Red, Blue, and Green) coordinates.

2.10. Reflectance spectra

The raw reflectance spectra of the untreated GSEP and GSEB and GSEP and GSEB exposed to white light and its red-orange, yellow-green-cyan, and cyan-blue-violet components at the maximum irradiation times were recorded at 1-nm resolution from 360 to 780 nm using a UV/VIS Lambda 35 spectrometer (PerkinElmer, USA) equipped with a Labsphere RSA-PE-20 integrating sphere.

2.11. Statistical analysis

All experiments were conducted in a minimum of triplicate, and the data are expressed as mean ± standard deviation. The results of the color analysis using the RBG system are an average of ten measurements. The experimental results were compared using one-way analysis of variance (ANOVA) and Tukey's test using IBM SPSS Statistics 24 to assess the difference between the means, with a value of $p < 0.05$ considered statistically significant.

3. Results and discussion

3.1. Encapsulation efficiency and selection of the beads

Fig. 1 shows the wet and dry red grape seed extract powder–based beads. When fresh, the beads appear as individual spherical shapes with smooth, shiny, and wrinkle-free surfaces. The colors vary between white and light brown, depending on the ratio between the white (SA, WPC) and red-brown–colored (GSEP) raw materials. The absence of WPC in the 1:0:1:100 beads resulted in translucent capsules compared to the opaque appearance of the beads containing WPC. As the amount of extract added increased, the brown color of the beads became more pronounced. Upon drying, the GSEB turned brown, the polymer gel shrank significantly, and bead aggregation could be observed.

Table 1 summarizes the total polyphenol contents of the dried control beads, GSEP, and GSEB, the encapsulation efficiency and the weight of dried GSEB resulting from each recipe (g). The encapsulation efficiency ranged from 75.19 % to 88.08 %, with no significant differences observed between values above 86 %. The lowest encapsulation efficiency was observed for the beads whose walls were entirely alginate (1:0:1:100). The hydroxyl and carbonyl groups in alginate can establish weak interactions, such as hydrogen bonds and Van der Waals forces, with the hydroxyl groups from the polyphenols in the grape seed extract (Pedrali et al., 2020). During the ionic gelation process, the spontaneous diffusion of GSEP from the beads into the calcium chloride solution may have occurred due to the porous nature of the alginate network and the water solubility of some polyphenols. Furthermore, the shrinkage of the beads during drying can cause gel syneresis and the expulsion of soluble polyphenols with the removed water (Pedrali, Scarafoni, Giorgi, & Lavelli, 2023).

In the presence of WCP, the anionic groups on the alginate molecules are linked to the cationic patches on the surfaces of the protein molecules (Zhang, Zhang, Zou, & McClements, 2016), forming a more compact three-dimensional network structure (Liu et al., 2023), thereby reducing the loss of polyphenols. Due to their multiple hydroxyl groups, the polyphenols from grape seeds show a special affinity for proteins, especially proline (Shi, Yu, Pohorly, & Kakuda, 2003). Because proline is abundant in whey protein concentrate, an increase in the encapsulation efficiency of WPC-containing beads is justified. In addition, the carboxyl groups of the tartaric, malic, or citric acids found in grape seed extract (Li et al., 2023) can form bonds with the amino groups in WPC and strengthen the hydrogel network. For example, adding 1 g of WPC (1:1:1:100) resulted in an improved encapsulation efficiency by 14.95 % compared to beads without WPC (1:0:1:100) enhancing it from 75.19 % to 86.43 %. WPC does not have a higher retention capacity for GSEP than alginate. As Table 1 shows, adding of 1 g of WPC to 1:1:1:100 beads to obtain 1:2:1:100 beads, increased the EE by 2.56 %, from 86.43 % to

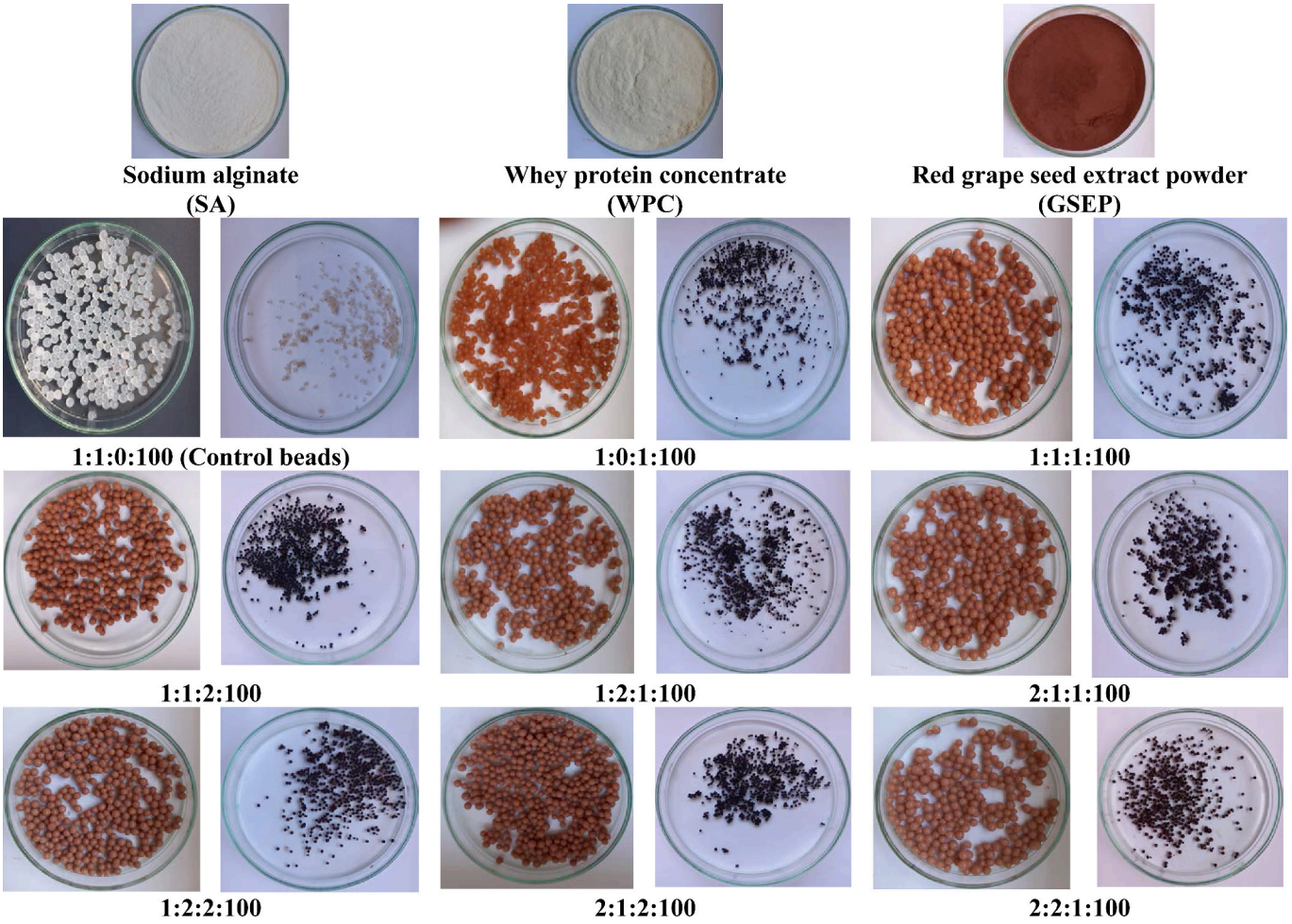

Fig. 1. Appearance of raw materials, dry and wet beads at different ratios of alginate:whey protein concentrate:red grape seed extract powder:water (w:w:w:v). (For interpretation of the references to color in this figure legend, the reader is referred to the web version of this article.)

88.64 %, although the results were not significantly different. When the 1:1:1:100 beads were enriched with 1 g of sodium alginate to produce 2:1:1:100 beads, the EE increased by only 1.00 % from 86.43 % to 87.29 %, again with no significant differences between the results.

In the case of beads with the same ratio of wall components, adding more GSEP did not result in higher encapsulation efficiency. The EE of 86.19 % obtained for 1:1:2:100 beads did not differ significantly from the EE of 86.43 % obtained for the 1:1:1:100 beads, with the excess GSEP removed during the rinsing of the beads. Yadav et al. (2019) has reported values of 58.25 % and 73.03 % for the encapsulation efficiency of GSE in whey protein concentrate and alginate, respectively. Pedrali et al. (2023) has reported an encapsulation efficiency of 82 % in pure alginate and 93 % in alginate combined with WPC to encapsulate the total polyphenols.

The beads prepared from SA:WPC:GSEP:water in the ratio 1:2:1:100 (w:w:w:v) were selected for further investigations because they had the most favorable encapsulation parameters in terms of the amount of total polyphenols (13.21 mg GAE/g), encapsulation efficiency (88.64 %), the smallest amount of GSEB obtained (4.85 g), and the lowest consumption of raw materials.

3.2. Morphology and microstructure of GSEB

The morphology of the beads can influence the release of the coated polyphenols and the pharmacodynamic and pharmacokinetic properties, affecting interactions with biological systems (Mutalik, Pandey, & Mutalik, 2020). Except for the sphericity factor, the beads shrank significantly in response to light (Table 2). Exposure to the white light

Table 2
Morphology of beads made from alginate-whey protein concentrate-red grape seed extract after light exposure.

Parameter	Unexposed	White light 30 min	Red-orange light 2 h 30 min	Cyan-blue-violet light 5 h 30 min	Yellow-green-cyan light 12 h
Area, mm^2	2.08 ± 0.22^{a}	1.93 ± 0.23^{d}	1.96 ± 0.22^{c}	2.01 ± 0.18^{b}	1.97 ± 0.28^{c}
Equivalent diameter, mm	1.63 ± 0.09^{a}	1.57 ± 0.10^{d}	1.58 ± 0.09^{c}	1.60 ± 0.07^{b}	1.58 ± 0.11^{c}
Maximum Feret diameter, mm	1.75 ± 0.10^{a}	1.69 ± 0.12^{d}	1.73 ± 0.11^{b}	1.72 ± 0.08^{c}	1.72 ± 0.13^{c}
Minimum Feret diameter, mm	1.56 ± 0.09^{a}	1.49 ± 0.10^{d}	1.49 ± 0.10^{d}	1.53 ± 0.09^{b}	1.51 ± 0.13^{c}
Perimeter, mm	5.93 ± 0.38^{a}	5.58 ± 0.35^{c}	5.66 ± 0.37^{bc}	5.70 ± 0.30^{b}	5.88 ± 1.07^{a}
Sphericity factor	0.06 ± 0.03^{a}	0.06 ± 0.03^{a}	0.07 ± 0.03^{a}	0.06 ± 0.03^{a}	0.07 ± 0.03^{a}

Results are expressed as average ± standard deviation (at least 30 beads of each type were used to quantify the shape parameters). In each row, the mean values marked with different superscript letters are significantly different ($p < 0.05$).

had the greatest effect on the area, equivalent diameter, maximum Feret diameter, and perimeter compared to those of the unexposed beads, with relative decreases of 7.21 %, 3.68 %, 4.49 %, and 5.90 %, respectively. The cyan-blue-violet light had the least influence on the area, equivalent diameter, and minimum Feret diameter, with relative decreases of 3.85 %, 1.44 %, and 1.92 %. The maximum Feret diameter was reduced by 1.14 % at the lowest extent by the red-orange light. The smallest decrease in the bead perimeter, 0.84 %, was observed upon exposure to yellow-green-cyan light, whereas the minimum Feret diameter had the highest reduction, 4.49 %, under exposure to white light and red-orange light.

These changes may relate to the water trapped inside the bead network. During the gelation process, the water molecules are retained by the Van der Waals attraction, hydrogen bonds, or ionic bonds. Under the influence of light, the energy level of the O—H bonds and their vibrational movements increase, potentially causing the hydrogen bonds between water molecules to weaken and break, shrinking the network. Furthermore, increasing the kinetic mobility of the polyphenol chains in the presence of reactive species (R•) (discussed in Section 3.3) could lead to chain breakage: shortened chains form and rearrange to form stronger bonds and a more densely packed core. Dehydration could also shrink the beads, but only in a small amount, because the temperature increases slightly until the end of the light exposure treatment. Exposure to light bands did not affect the sphericity of the beads

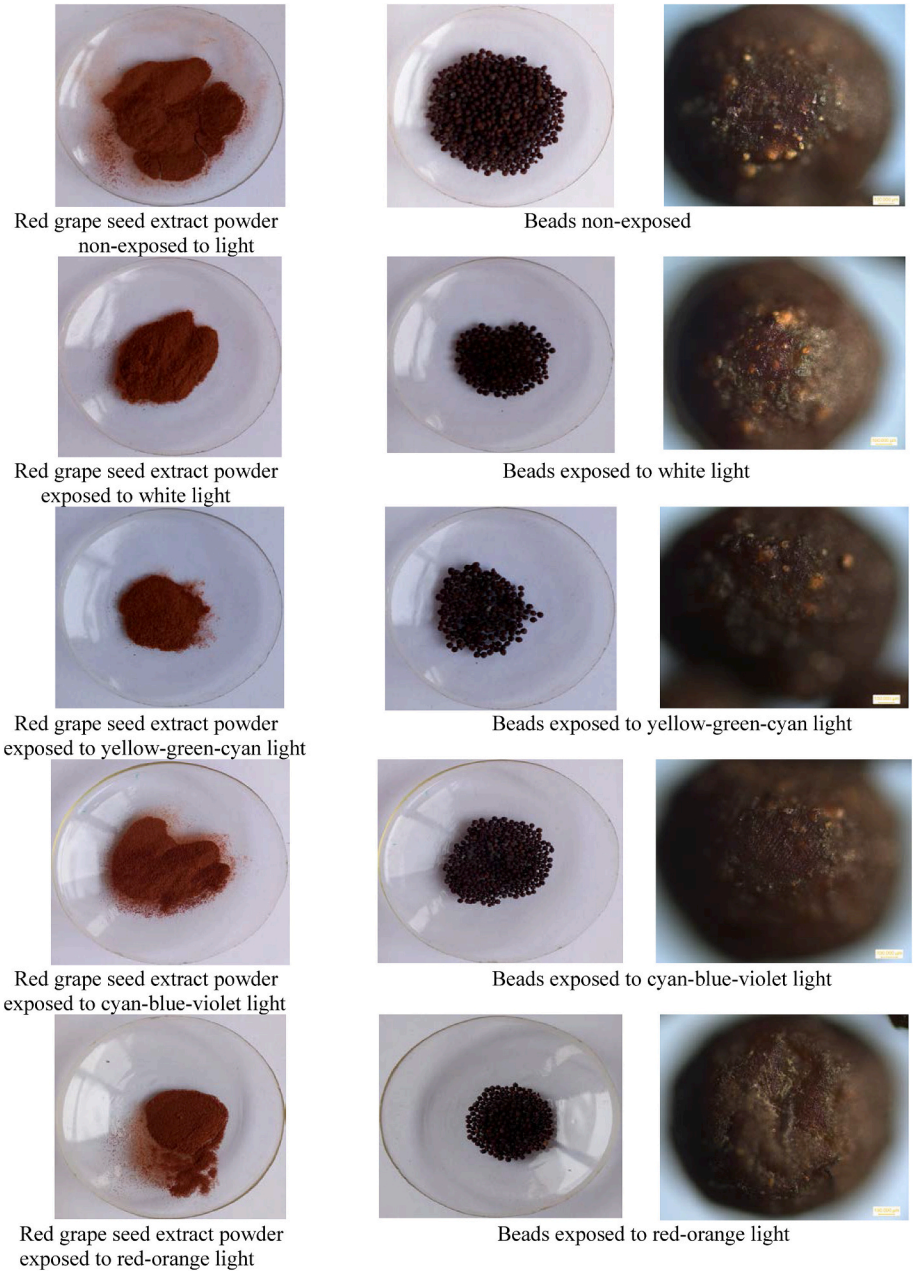

Fig. 2. Appearance and Red, Blue and Green (RBG) color coordinates of red grape seed extract powder (GSEP) and red grape seed extract beads (GSEB) unexposed and after exposure to white light, yellow-green-cyan light, cyan-blue-violet light, and red-orange light:
a. Digital photographs; b. Scanning electron microscope (SEM) images of shell and core of beads; c. RBG coordinates associated to GSEP; d. RBG coordinates associated cu GSEB; the values between the RBG coordinates, as well as between the treatments are significantly different ($p < 0.05$); the standard deviations of values ranged from 0.0307 to 0.0897 in GSEP, and from 0.0032 to 0.0070 in GSEB. (For interpretation of the references to color in this figure legend, the reader is referred to the web version of this article.)

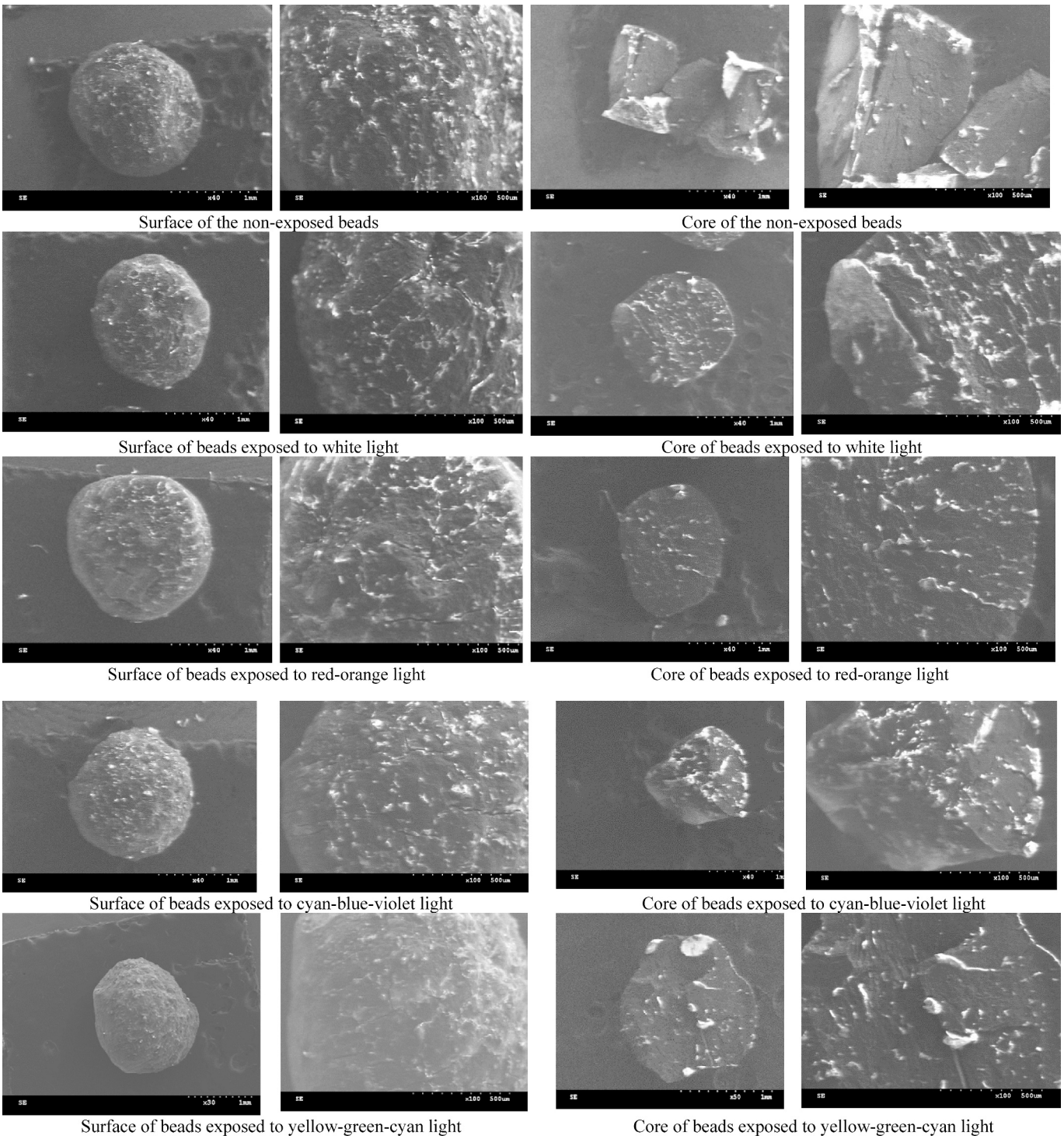

Fig. 2. (*continued*).

compared to unexposed beads; no statistical differences were observed.

The digital photographs and SEM images of the beads are shown in Figs. 2a,b,c. The 40× and 100× magnifications were used to obtain SEM images to facilitate characterization of the surface and core. For unexposed beads, a round shape without bursts, punctures, or concavities, with a granular surface, probably due to the granular structure of the extract powder, was observed. The core has a rough, compact, and cohesive structure. The fine cracks observed in the shell and core could be due to the bead drying process.

After light exposure, the beads remained spherical, although they were slightly less regular with a coarser morphology. The cracks in the shell became deeper, more numerous, and visible. There was no propagation of cracks into the core of the beads exposed to white light, red-orange light, and yellow-green-cyan light. Larger and deeper cracks were visible in the core of beads exposed to cyan-blue-violet light, suggesting a stronger structural rearrangement due to dehydration or depolymerization of polyphenol chains.

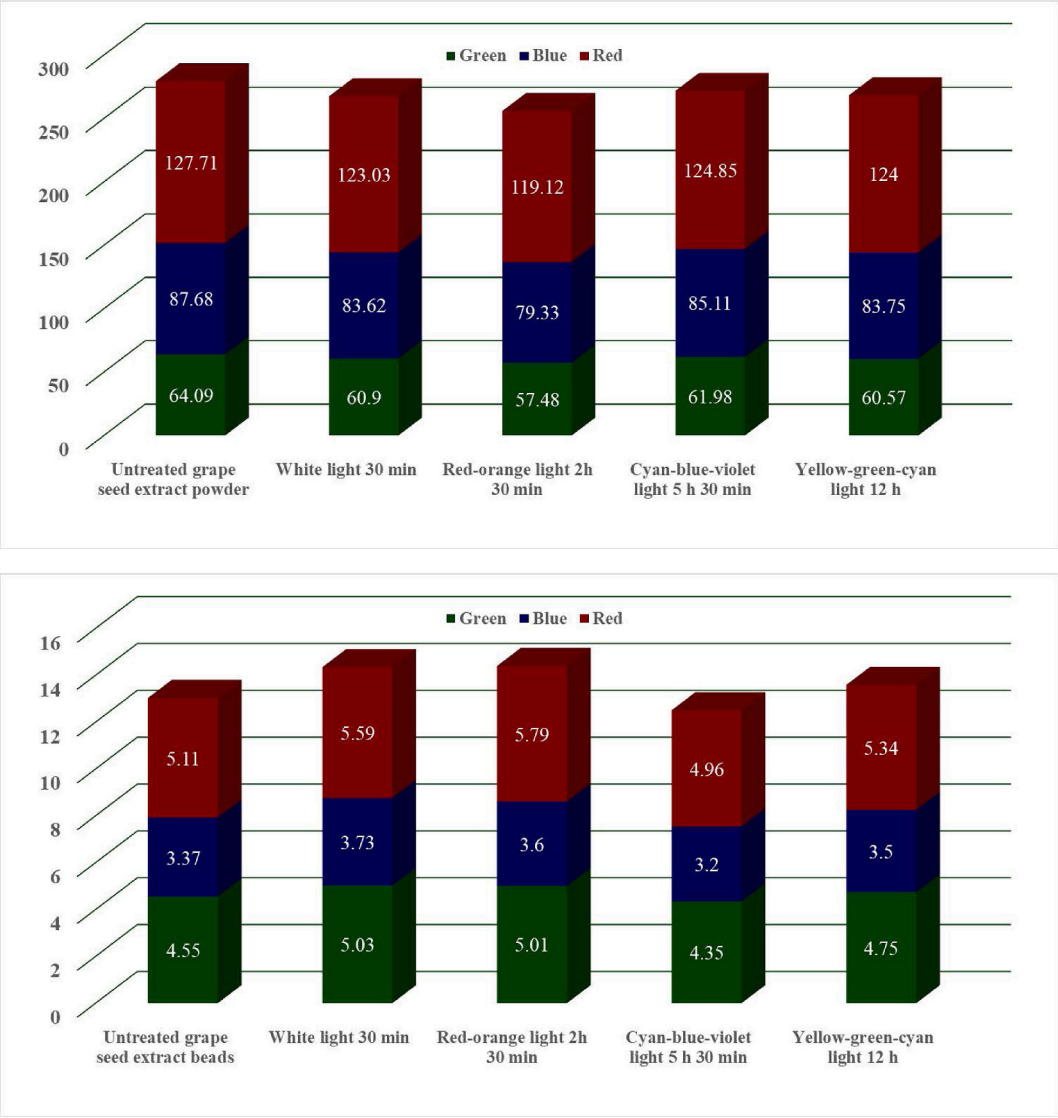

Fig. 2. (*continued*).

3.3. Quantification of total polyphenols and flavonoids

The total polyphenol and flavonoid concentrations in the GSEP and GSEB exposed to white light and its red-orange, yellow-green-cyan, and cyan-blue-violet illuminants in the visible region are summarized in Table 3. Reductions in the TPC were observed in both GSEP and GSEB. After exposure to white light, yellow-green-cyan light, and red-orange light, statistically significant differences ($p < 0.05$) between the TPCs of GSEP and GSEB were measured: the highest values occurred in GSEB, demonstrating the shielding effect of the alginate–whey matrix. In the case of cyan-blue-violet light, no statistically significant differences in the TPCs were observed between GSEP and GSEB, either during exposure or at the end, which does not recommend encapsulation. The ranking of the impact of the investigated lights on the TPC yields the series white light (8.86 %) < cyan-blue-violet light (11.54 %) < yellow-green-cyan light (11.90 %) < red-orange light (13.18 %) for GSEP, and white light (4.34 %) < yellow-green-cyan light (8.21 %) < cyan-blue-violet light (8.90 %) < red-orange light (9.48 %) for GSEB.

Regarding the TFC in GSEP, significant differences ($p < 0.05$) between the initial and final amounts occurred only with exposure to yellow-green-cyan light, white light, and cyan-blue-violet light. In the case of red-orange light, the differences were noted at the maximum exposure time and immediately prior. The flavonoids in GSEB were not affected by exposure to yellow-green-cyan light or white light, with experimental results showing no significant differences between the initial and final results. The impact of the investigated lights on flavonoids resulted in the series yellow-green-cyan light (9.19 %) < white light (11.13 %) < cyan-blue-violet light (12.05 %) < red-orange light (15.82 %) for GSEP, and yellow-green-cyan light (8.31 %) < white light (9.46 %) < cyan-blue-violet light (9.99 %) < red-orange light (10.70 %) for GSEB. Regarding flavonoid protection, the encapsulation of red grape seed extract powder was not justified for exposure to white light, cyan-blue-violet light, and yellow-green-cyan light. The flavonoid concentrations in GSEP and GSEB did not differ significantly during or after exposure. The protective effect of the alginate–whey protein concentrate matrix was expressed against red-orange light at the end of exposure, with a flavonoid content in GSEB 5.73 % higher than that of GSEP ($p < 0.05$).

The interactions between the polyphenols and white light or its component illuminants could explain the decrease in TPC and TFC. Generally, polyphenols are both reducing and pro-oxidating agents, depending on their structural characteristics and the electronic configuration of the hydroxyl oxygen attached to the benzene ring. Some polyphenols absorb the photons of light of a particular wavelength

Table 3
Total polyphenol and flavonoid contents in red grape seed extract powder (GSEP) and selected red grape seed extract-based beads (GSEB) upon exposure to light.

Exposure	Duration of exposure	Total polyphenols in GSEP, mg GAE/g powder	Total polyphenols in GSEB, mg GAE/4.85 g beads	Total flavonoids in GSEP, mg CE/g powder	Total flavonoids in GSEB, mg CE/4.85 g beads
White light	Unexposed	723.52 ± 22.50^{ai}	723.52 ± 22.50^{ai}	172.34 ± 8.39^{ai}	172.34 ± 8.39^{ai}
	3 min 45 s	719.23 ± 18.34^{ai}	721.01 ± 16.37^{ai}	169.35 ± 6.84^{abi}	170.02 ± 7.53^{ai}
	7 min 30 s	690.15 ± 13.94^{abi}	699.29 ± 14.96^{ai}	161.14 ± 6.25^{abi}	164.12 ± 6.27^{ai}
	15 min	670.33 ± 14.21^{bi}	690.38 ± 14.57^{ai}	155.22 ± 6.21^{abi}	159.09 ± 6.38^{ai}
	30 min	659.45 ± 13.19^{bj}	689.39 ± 13.10^{bi}	153.16 ± 6.19^{bi}	156.03 ± 6.24^{ai}
Red-orange light	Unexposed	723.52 ± 22.50^{ai}	723.52 ± 22.50^{ai}	172.34 ± 8.39^{ai}	172.34 ± 8.39^{ai}
	16 min 15 s	688.25 ± 20.65^{abi}	698.08 ± 20.73^{abi}	167.22 ± 5.85^{ai}	170.35 ± 5.11^{ai}
	32 min 30 s	662.89 ± 16.84^{bci}	677.01 ± 20.38^{abi}	160.01 ± 3.55^{abi}	165.44 ± 4.04^{abi}
	1 h 15 min	639.66 ± 19.91^{cj}	662.33 ± 9.93^{bi}	152.13 ± 3.09^{bcj}	159.81 ± 3.34^{abi}
	2 h 30 min	620.15 ± 14.82^{cj}	653.90 ± 15.00^{bi}	145.09 ± 2.76^{cj}	153.90 ± 4.65^{bi}
Cyan-blue-violet light	Unexposed	723.52 ± 22.50^{ai}	723.52 ± 22.50^{ai}	172.34 ± 8.39^{ai}	172.34 ± 8.39^{ai}
	41 min 15 s	698.78 ± 20.96^{abi}	702.34 ± 21.07^{abi}	168.18 ± 6.73^{abi}	168.18 ± 6.71^{ab}
	1 h 22 min 30 s	663.64 ± 14.09^{bci}	680.29 ± 15.85^{abi}	165.44 ± 6.97^{abi}	165.44 ± 5.89^{ab}
	2 h 45 min	650.11 ± 16.64^{ci}	674.88 ± 16.60^{abi}	159.23 ± 5.02^{abi}	159.23 ± 5.97^{ab}
	5 h 30 min	631.04 ± 14.77^{ci}	659.12 ± 15.56^{abi}	151.58 ± 5.88^{bi}	155.13 ± 4.59^{bi}
Yellow-green-cyan light	Unexposed	723.52 ± 22.50^{ai}	723.52 ± 22.50^{ai}	172.34 ± 8.39^{ai}	172.34 ± 8.39^{ai}
	1 h 30 min	700.23 ± 13.44^{abi}	702.39 ± 21.28^{abi}	170.02 ± 6.27^{abi}	171.56 ± 7.60^{ai}
	3 h	670.11 ± 13.94^{bci}	684.44 ± 13.76^{abi}	162.76 ± 4.88^{abi}	165.52 ± 6.69^{ai}
	6 h	657.18 ± 14.26^{ci}	675.03 ± 13.30^{bi}	158.92 ± 6.37^{abi}	160.02 ± 4.98^{ai}
	12 h	637.45 ± 11.28^{ci}	664.11 ± 11.75^{bj}	154.50 ± 6.20^{bi}	158.02 ± 5.10^{ai}

a-c lowercase superscript letters in the same column of each treatment are significantly different ($p < 0.05$); i and j lowercase superscript letters in the same row for the same parameter are significantly different ($p < 0.05$); the total polyphenol concentrations in the beads are expressed as mg GA/4.85 g beads, where 4.85 g is the weight of beads obtained from selected recipe (see Table 1).

depending on their optical properties and enter an excited singlet state with a short life or an excited triplet state (T_1) with a longer life due to the electronic transition between π-type molecular orbitals (Anouar, Gierschner, & Duroux, & Trouillas, 2012). When they return to the ground state, the energy is transferred to an oxygen molecule, generating reactive oxygen species (ROS), such as H_2O_2, O_2^{-1}, HO^- or $^1O_2$. Other polyphenols, due to the increased tautomeric effects of the intra- or intermolecular H-bonding on the O—H groups around the benzene ring, generate four forms of resonance for the phenol molecule, three as hydroquinone cation radicals containing an unpaired electron in the ortho-, meta- or para-positions of the benzene ring, and one, the regular structure (Foti, 2007; Galleano, Verstraeten, Oteiza, & Fraga, 2010). These new structures can decrease the bond dissociation enthalpy of the O—H bond and increase the reducing activity of the molecule. The electronic configuration of the hydroquinone cation radical allows direct interactions with oxygen molecules that generate ROS, such as H_2O_2, HOO•, $O_2^{-\bullet}$, quinones, and semi-quinones.

Due to a combination of electronic and steric effects, some polyphenols are more active than others, and in the presence of reactive species (R•), continue the chain reaction, generating more reactive species according to the reactions (Kanner, 2020):

$$Ph - OH + (R\bullet) \rightarrow Ph - O\bullet + \text{reduced compounds} \quad (1)$$

$$Ph - O\bullet + O_2 \rightarrow Ph = O + O_2\bullet^- \quad (2)$$

$$Ph - O\bullet + O_2\bullet^- \rightarrow Ph = O + H_2O_2 \quad (3)$$

$$Ph - OH + Ph = O \rightarrow 2Ph - O\bullet \quad (4)$$

If the phenoxy radical is not sufficiently stable in a mixture with other polyphenols, for example in grape seed extract, will continue the chain reaction by attacking another polyphenol molecule (Kanner, 2020):

$$Ph - O\bullet + Ar - OH \rightarrow Ph - OH + Ar - O\bullet \quad (5)$$

In contrast, some polyphenols act as scavengers of ROS and thus interrupt the chain reactions. The riboflavin, catechol, and galloyl group (gallic acid, chlorogenic acid, caffeic acid, protocatechuic acid), which can be found in grape seed extract, have been reported to be efficient ROS generators (Kanner, 2020). In contrast, due to their high tendency to donate H-atoms from their hydroxyl group at position 4′, rutin and catechin play dual roles as ROS scavengers and deactivators of the triplet excited state riboflavin quenchers, respectively (Ji & Shen, 2008).

The lower or higher impact of different illuminants on TPC and TFC in GSEP and GSEB resulted from the combined effects of the sample composition, energy provided to the sample by each illuminating band, and absorbed photon energy. Even if they are high energy, the yellow-green-cyan and cyan-blue-violet light were absorbed only in small amounts. Red-orange light, characterized by lower energy, was absorbed in a larger amount and affected the TPC and TFC more strongly. In some cases, the alginate–whey protein matrix contributed to protecting the TPC and TFC. Despite their maximum absorption peaks in UV domain at 265 nm and 280 nm, the matrix can absorb small amounts of energy from incident VIS light and reduce the energy transferred to the encapsulated extract.

3.4. Quantification of cyanidin-3-O-glucoside

As the results in Table 4 show, cyanidin-3-*O*-glucoside deteriorated when exposed to light, likely due to the hydrolysis of the carbon atom at position C2, which opens its pyrylium ring and produces a chalcone structure (Norman, Bartczak, Zdarta, Ehrlich, & Jesionowski, 2016). In

Table 4
Total cyanidin content in red grape seed extract powder (GSEP) and selected red grape seed extract beads (GSEB) after light exposure.

Exposure	Exposure time	Cyanidin 3-*O*-glucoside in GSEP, μg/g powder	Cyanidin 3-*O*-glucoside in GSEB, μg/4.85 g beads
Non-exposed	–	4143.92 ± 204.40^{ae}	4207.15 ± 161.12^{ae}
White light	30 min	3094.12 ± 123.87^{bf}	3456.22 ± 114.90^{be}
Red-orange light	2 h 30 min	3355.73 ± 128.78^{bf}	3780.01 ± 151.24^{be}
Cyan-blue-violet light	5 h 30 min	2195.10 ± 86.20^{ce}	2201.77 ± 126.50^{de}
Yellow-green-cyan light	1 h 30 min	2094.12 ± 93.16^{cf}	3024.52 ± 107.35^{ce}

a-d lowercase superscript letters in the same column for each exposure are significantly different ($p < 0.05$); e and f lowercase superscript letters in different rows for the same exposure are significantly different ($p < 0.05$); the cyanidin 3-*O*-glucoside concentrations in the beads are expressed as mg GA/4.85 g beads, where 4.85 g is the weight of beads resulted from selected recipe (see Table 1).

GSEP, the most consistent response was caused by the yellow-green-cyan and the cyan-blue-violet lights, which reduced the C3G concentration by 49.47 % and 47.03 %, with no significant differences between the results. The C3G in GSEP is less sensitive to white and red-orange lights, with concentrations reduced by 25.33 % and 19.02 %, respectively, with no significant differences between the results. Similar trends were observed for the C3G content of GSEB, with decreases of 47.67 % and 28.11 % under cyan-blue-violet light and yellow-green-cyan light, respectively, and 17.85 % and 10.15 % under red-orange light and white light. The predominant light absorption from blue to green explains the strongest impact of yellow-green-cyan and cyan-blue-violet light bands on C3G. Except for the exposure to cyan-blue-violet light, the exposure to the other light bands caused less effect on the cyanidin-3-*O*-glucoside in GSEB compared to GSEP, proving that it has higher stability under encapsulation due to the protection from oxidation provided by the alginate–whey protein matrix. C3G does not appear to be stable due to encapsulation upon exposure to cyan-blue-violet light: its concentration in GSEB did not differ significantly compared to GSEP. As in the case of TPC and TFC, encapsulation of red grape seed extract in alginate–whey protein concentrate did not protect C3G from degradation upon exposure to cyan-blue-violet light. Our results are consistent with the literature reporting the stabilization of C3G encapsulated in casein or lecithin and cholesterol nanoliposomes under the action of white light, oxidation, and thermal treatment (Chi et al., 2019; Ouyang et al., 2020).

3.5. Color analysis

The results of the color analysis (Fig. 2d) show that the brownish-red color of the untreated GSEP results mainly from the presence of red components (127.71) mixed with blue (87.68) and green (64.09) components. Regarding the GSEB, the dark brown color results from a combination of much lower R(5.11), B(3.37), and G(4.55) values, which results from the dilution of grape seed extract with alginate, whey proteins, and water during encapsulation. The red compounds dominate the GSEB, but there are fewer blue compounds than green ones, unlike GSEP, probably due to the white color of the raw materials used in the matrix. The dominance of red compounds is consistent with the chemical analysis indicating high amounts of cyanidin 3-*O*-glucoside, the red compound dominant in red grape seed.

The exposure to light bands affected the color of the extract powder, which can be expressed by comparing individual RBG coordinates to their initial values, which indicates polyphenol degradation. The lowest values of the RBG color coordinates in GSEP were obtained from exposure to red-orange light, 119.12 for R, 79.33 for B, and 57.48 for G. Compared to untreated GSEP, the reductions were 6.73 % for red, 9.99 % for blue, and 10.31 % for green, corresponding to an average RBG reduction of 8.43 %. The 30-min white light exposure of GSEP reduced the total RBG coordinates by 4.27 %, resulting from reductions in R, B, and G coordinates of 3.67 %, 4.63 %, and 4.98 %, respectively. After 12 h of exposure to yellow-green-cyan light, the RBG triplet was reduced by 3.99 %. The R coordinate accounted for the lowest reduction with 2.91 %, followed by G at 5.49 % and B at 4.48 %. Exposure to cyan-blue-violet light for 5 h 30 min had the least impact on RBG coordinates, accounting for 2.24 %, 2.93 %, and 3.29 % for the RBG triplet, with an average of 2.70 %.

The response of GSEB differed from that of GSEP during the light exposures (Fig. 2e). Except for exposure to cyan-blue-violet light, the intensity of the reddish shade increased. The highest value for the R coordinate, 5.79, was observed under red-orange light. Under cyan-blue-violet light, the R-value significantly decreased ($p < 0.05$) by 2.84 %. These variations are consistent with the principle of absorption of complementary radiation. Red compounds absorb blue-to-green radiation and concentrate complementary color compounds due to their structural changes. Contrary to the principle of absorption of complementary radiation, the intensity of blue compounds increased significantly ($p < 0.05$) under all lights except cyan-blue-violet. In addition, the intensity of the R coordinate decreased under exposure to cyan-blue-violet light and increased when GSEB was exposed to the other colored lights. These seemingly contradictory variations can be explained by an additional process: the release of bound polyphenols. Under the cyan-blue-violet or red-orange lights, the polyphenols bound in structures without absorption in the visible (VIS) domain were released and expressed their spectral features in the VIS range, explaining the higher measured R values.

The sums of RBG triplet also display different trends in GSEP and GSEB (Fig. 2d and e). For GSEP, the decrease in the RBG sum after exposure to lights compared to unexposed GSEP suggests that the polyphenol content decreased. For GSEB, exposure to cyan-blue-violet light decreased the RBG sum, whereas exposure to white, red-orange, and yellow-green-cyan lights resulted in increased RBG sums, suggesting the accumulation of free polyphenols, which is probably due to their release from bound-polyphenol structures. The RBG sums of the GSEP and GSEB exposed to cyan-blue-violet light decreased with identical values of 3.99 % compared to unexposed correspondent samples, indicating that the encapsulation of red grape seed extract is not supported. This agrees with the conclusion drawn from analyses of total polyphenols, flavonoids, and cyanidin-3-*O*-glucoside, which did not recommend encapsulation of grape seed extract in an alginate–whey protein concentrate matrix because the differences between TPC, TFC, and C3G in GSEP and GSEB under exposure to cyan-blue-violet light were statistically insignificant.

3.6. Reflectance spectra

3.6.1. Deconvolution of reflectance spectra

Deconvolution of reflectance spectra was conducted for qualitative and semi-quantitative screening of optically active compounds in untreated and treated GSEP and GSEB. The procedure, illustrated on the raw spectrum associated with untreated GSEP, required the following steps:

(1) Savitzky–Golay filtering was applied to the acquired raw reflectance spectrum to remove background noise, using a third-order polynomial with a 25-point window. The baseline level of the filtered spectrum was zeroed with regard to the minimum reflection values. All spectra associated with light exposure displayed a similar shape. The analysis of the unexposed GSEP filtered spectrum (Fig. 3a) indicates that the shift towards higher wavelengths is accompanied by higher reflectance values, with the color analysis also demonstrating the dominance of red compounds. Visually, in the GSEP and GSEB reflectance spectra, six or seven groups of colored compounds were identified (not always accurate), corresponding to the wavelengths for which the spectra showed local peaks.
(2) The accurate wavelength characteristics of the colored compound groups were extracted from the second-order derivative profile obtained after applying the Savitzky–Golay coefficients for a third-order polynomial with a 25-point window. Fig. 3b shows the second-order derivative profile computed from the filtered reflectance spectrum of unexposed GSEP. The seven minimum values around 405, 455, 509, 565, 626, 680, and 716 nm extracted from Fig. 3b correspond to the family of colored compounds in the GSEP samples (Table 5). Only six minimum values were identified in the GSEB samples, positioned at 404, 456, 508, 568, 621, and 676 nm (Table 5). Only small amounts of compounds associated with the reflectance wavelength at 717 nm in the unexposed GSEP appear to be present, considering the low peak area value of 53.68. Their absence in the corresponding GSEB sample can be explained by dilution during encapsulation of the powder extract with alginate and whey or by the formation of complexes with whey–alginate, which are inactive in VIS domain. Compared to color analysis, which indicates the

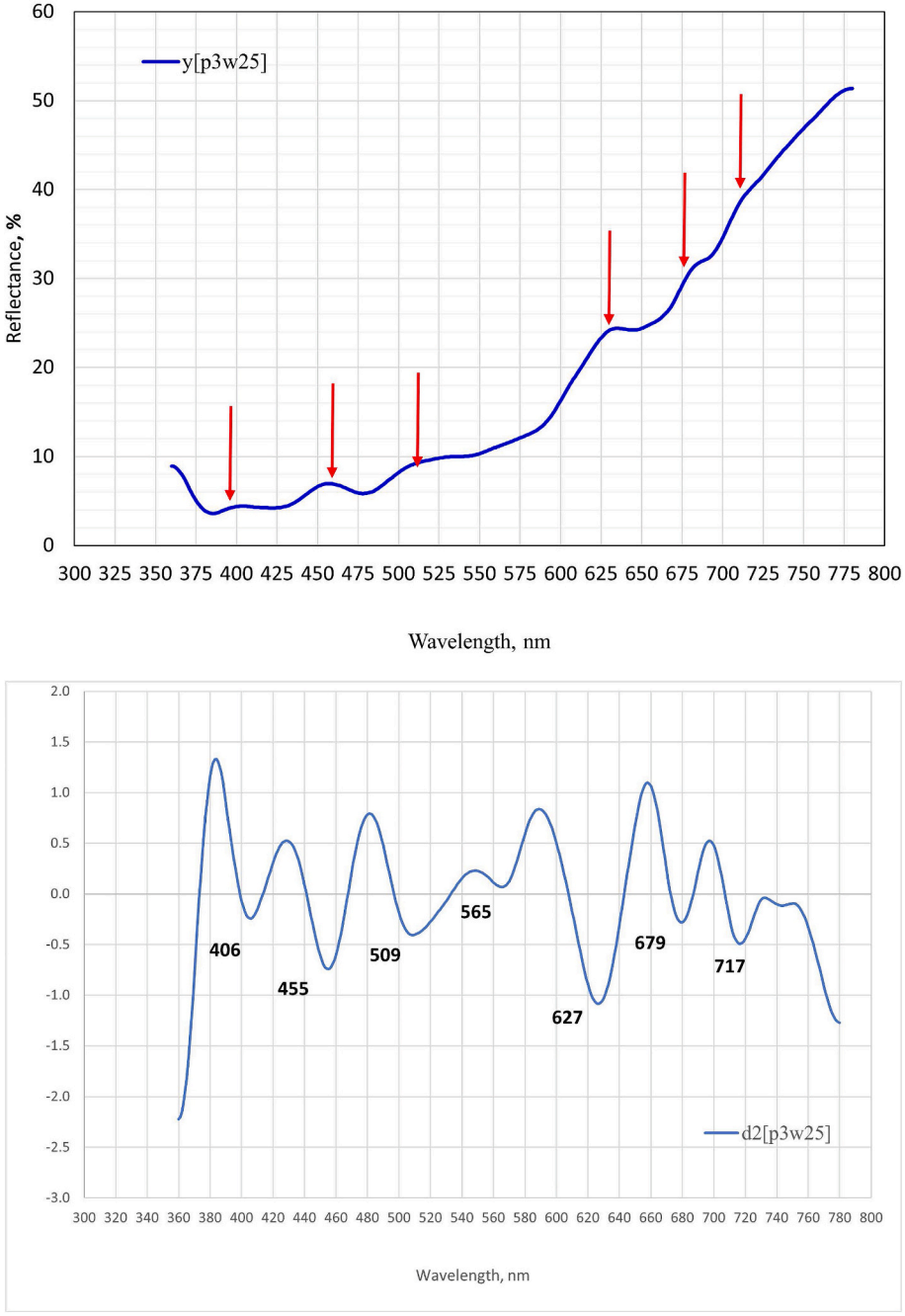

Fig. 3. Processing of raw reflectance spectrum illustrated for unexposed red grape seed extract powder (GSEP):
a. Filtered reflectance spectrum; b. Second-order derivative of filtered reflectance spectrum; c. Deconvolution of filtered spectrum; y – raw spectrum; g1-g9 – deconvolved Gaussian distributions, y(sum) - sum of the Gaussian distributions. (For interpretation of the references to color in this figure legend, the reader is referred to the web version of this article.)

presence of three groups of colored compounds using the RBG sum, the second-order derivative of filtered reflectance spectra differentiated seven (GSEP) or six (GSEB) families of colored compounds, indicating the composition of the samples more accurately.

Typically, two absorption clusters appear in the UV-VIS spectrum of anthocyanins in the region 260–280 nm in the UV band and 490–550 nm in the VIS region (Saha, Singh, Paul, & Sarkar, 2020; Chowdhuri et al., 2021). Due to the complementarity of absorption and transmittance of light, the first region did not correspond to the reflectance in the visible region, while the second region corresponds to the reflectance region around 400–620 nm. The literature reports that methylated anthocyanins are associated with a hypsochromic shift in their absorption towards lower wavelengths. The more pronounced the methylation is, the lower the absorption wavelength (cyanidin→peonidin→malvidin) (Saha et al., 2020). However, the acylated anthocyanins undergo a bathochromic shift in absorption to higher wavelengths, where an increase in the number of substituted hydroxyl groups accompanies the higher absorption (pelargonidin → cyanidin → delphinidin) (Anouar et al., 2012). As a result of these hypsochromic and bathochromic effects, overlapping of the reflectance spectra of methylated anthocyanins and acylated

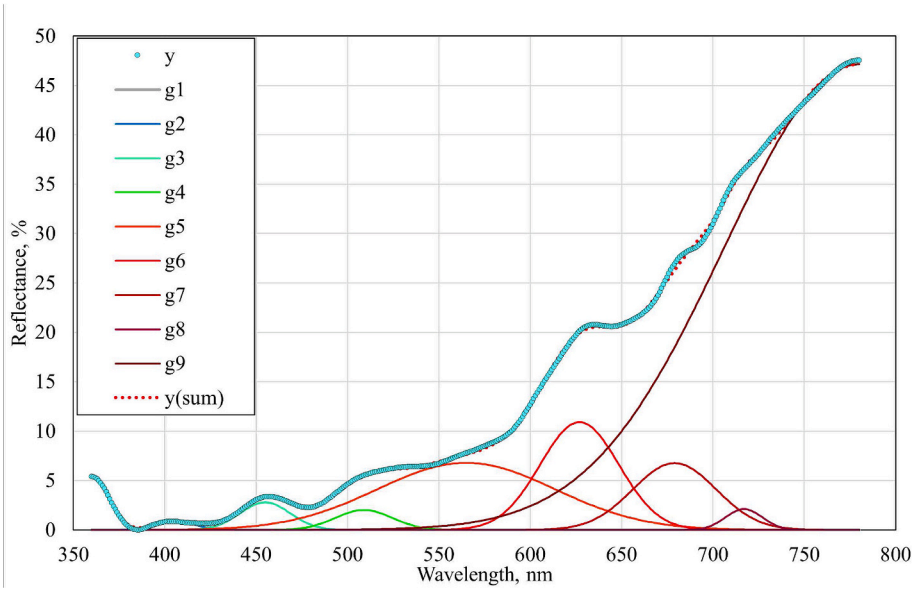

Fig. 3. (*continued*).

anthocyanins might occur around 670 nm.

The reflectance band at 520–600 nm indicates the presence of sugar moieties attached to the anthocyanidin moiety, whose absorption occurred in the 400–450 nm range (Saha et al., 2020). Polymeric anthocyanins were identified at 565 nm, suggesting self-association complexes because of the hydrophilic interactions between the glucose components of the corresponding anthocyanin molecules and the hydrophobic repulsion between their aromatic nuclei and water (González-Manzano, Santos-Buelga, Dueñas, Rivas-Gonzalo, & Escribano-Bailón, 2008). This special co-pigmentation of anthocyanins has been reported to produce a hypsochromic effect (González-Manzano et al., 2008). The absorption of protein–tannin complexes at around 509 nm (Aleixandre-Tudo & du Toit, 2018), corresponds to the 670–717 nm reflectance band. In addition to anthocyanins, the reflectance at 550–650, 700–710, and around 680 nm corresponds to chlorophyll *a* (Gitelson & Merzlyak, 1996; Merzlyak, Solovchenko, & Gitelson, 2003). The absorption peaks around 627 nm and reflected around 450 nm could arise from chlorophyll *b* (Giovenzana, Civelli, Beghi, Oberti, & Guidetti, 2015). Due to their various chemical structures, anthocyanins are found in all seven groups of colored compounds.

The minimum values of the second-order derivative are also displayed for the minimum and maximum of the wavelength range, 360 and 780 nm. In the VIS spectrum, they correspond to inactive compounds not involved in coloring the samples. For each previously determined wavelength, a Gaussian distribution was considered, characterized by a specific gain factor and a standard deviation value, both of which were initialized to 1 in the iterative deconvolution algorithm. For each wavelength of the reflectance spectrum in the range 360–780 nm, at a resolution of 1 nm, the reflectance was calculated as the sum of the reflectance of each component associated with the Gaussian distribution and the sum of the square differences (SS) between them and the corresponding spectrum values. Applying the Generalized Reduced Gradient nonlinear optimization method (Microsoft Office, Excel), the optimal values of the multiplication factors and standard deviations of the considered distribution were calculated to ensure minimum SS(%) values. The values of the multiplication factors correspond to the distribution areas considered characteristics of the optically active-colored compounds in the samples. Each deconvolution was run for 10 repetitions for untreated and treated samples.

The lowest values for the squared correlation coefficients between the reflection spectra and the sum spectra of the component distribution were 0.9998, while the SS(%) was 0.0112 %. These low values validate the deconvolution process. The values corresponding to the optically active compounds in the samples were subjected to inappropriate data removal tests, after which the mean and standard deviation values were calculated on a case-by-case basis (Table 5). Testing for extreme values was performed using the Grubbs test. The post-test variability results showed a relative standard deviation ranging from 0.15 % to 7.79 %, corresponding to an average mean of 2.56 %. As an example, Fig. 3c shows the deconvolution of the filtered spectrum presented in Fig. 3a.

3.6.2. *Analysis of deconvoluted reflectance spectra*

In the case of the unexposed GSEP, the highest peak area occurred at 565 nm (Table 5). This group remained predominant regardless of the exposure type. The analysis of the peak areas of treated GSEP indicates that, with one exception, the peak areas corresponding to the wavelengths of colored compound families have lower values than those of untreated GSEP, confirming the degradation of polyphenols suggested by the chemical analysis. The exception relates to GSEP exposed to red-orange light, where the peak area of 434 corresponding to 679 nm was slightly higher than the value 398.16 of the unexposed GSEP at the same wavelength, although the results were not significantly different. This difference might suggest that the colored compounds originating from other groups undergo structural changes after absorbing red-orange light, resulting in red-colored compounds whose characteristic wavelength is shifted towards 679 nm. The seven groups of colored compounds in GSEP are differently affected by the types of light to which they were exposed (Table 5). The highest and lowest impact of white light is seen for the compounds at 717 and 679 nm, with peak areas reduced by 27.09 % and 5.53 %, respectively. The red-orange light reduced the peak area at 627 nm the least and that at 717 nm the most, although there was an increase in peak area for the compounds at 679 nm. The compounds at 719 nm were also reduced by the cyan-blue-violet light the most, 37.51 %, while those at 406 nm were reduced the least, 3.16 %. Under yellow-green-cyan light, reductions ranging from 2.36 % for the compounds at 679 nm to 28.92 % for compounds at 717 nm were recorded. Considering the spectral component of the four types of light used for exposure, the results are consistent with the principle of absorption of complementary radiation.

The evolution of the peak areas assigned to the six colored groups in GSEB is shown in Table 5. The lowest areas were obtained from cyan-blue-violet light exposure, which could be considered the most likely

Table 5
Areas of peaks from the deconvoluted reflectance spectra corresponding to colored compound groups in unexposed GSEP and GSEB, and GSEP and GSEB after light exposure.

The peak areas [R(%)·nm]						
Red grape seed extract powder (GSEP)						
Wavelength, nm	Compounds	Unexposed	Exposed to white light	Exposed to red-orange light	Exposed to cyan-blue-violet light	Exposed to yellow-green-cyan light
406	anthocyanins (Saha et al., 2020)	21.35±0.36^{a}	19.71±0.31^{c}	16.82±0.01^{d}	20.67±0.03^{b}	19.17±0.23^{c}
455	anthocyanins (Saha et al., 2020) chlorophyll *b* (Giovenzana et al., 2015)	95.45±0.79^{a}	84.68±1.11^{b}	80.16±5.46^{b}	86.82±1.15^{b}	83.08± 0.27^{b}
509	anthocyanins (Saha et al., 2020)	77.61±1.11^{a}	65.94±0.46^{c}	57.69±0.68^{d}	70.56±2.70^{b}	63.67±0.85^{c}
565	polymeric anthocyanins (Chowdhuri et al., 2021) sugar-anthocyanidin moieties (Saha et al., 2020) chlorophyll *a* (Gitelson and Merzlyak, 1996)	833.04±7.32^{a}	766.02± 4.22^{c}	692.01±1.06^{d}	788.29±6.86^{b}	778.01± 3.34^{bc}
627	anthocyanins (Chowdhuri et al., 2021) chlorophyll *a* (Gitelson and Merzlyak, 1996)	598.28±8.33^{a}	535.04±13.11^{b}	534.62±9.50^{b}	537.36±14.07^{b}	544.58±12.00^{b}
679	methylated anthocyanins (Saha et al., 2020) acylated anthocyanins (Saha et al., 2020) protein-tannins complexes (Aleixandre-Tudo and du Toit, 2018) chlorophyll *a* (Merzylak at al., 2003)	398.16±18.73^{ab}	376.15±28.46^{b}	434.00± 8.56^{a}	346.43±21.40^{b}	388.75±17.29^{ab}
717	anthocyanins (Chowdhuri et al., 2021) protein-tannins complexes (Aleixandre-Tudo and du Toit, 2018) chlorophyll *a* (Gitelson and Merzlyak, 1996)	53.68±2.39^{a}	39.14±2.36^{bc}	40.57±3.20^{b}	33.54±1.87^{c}	38.15±1.92^{bc}
Sum of peaks areas, [R(%)·nm]		2077.57	1886.68	1855.57	1883.67	1915.41
Red grape seed extract powder beads (GSEB)						
404	anthocyanins (Saha et al., 2020)	80.35±0.48^{b}	83.92±0.82^{a}	73.88±0.88^{c}	66.14±0.26^{d}	74.01± 0.13^{c}
456	anthocyanins (Saha et al., 2020) chlorophyll *b* (Giovenzana et al., 2015)	304.64±1.20^{d}	335.18±2.51^{a}	323.38±1.48^{b}	279.62±1.05^{e}	310.82±1.88^{c}
508	anthocyanins (Saha et al., 2020)	327.74± 2.45^{d}	376.85±3.72^{a}	370.29±1.33^{b}	312.92±0.89^{e}	353.32±1.04^{c}
568	polymeric anthocyanins (Chowdhuri et al., 2021) sugar-anthocyanidin moieties (Saha et al., 2020) chlorophyll *a* (Gitelson and Merzlyak, 1996)	1773.41± 8.78^{c}	1898.45±8.80^{b}	1933.27±5.48^{a}	1630.52±2.51^{d}	1771.57±3.57^{c}
621	anthocyanins (Chowdhuri et al., 2021) chlorophyll *a* (Gitelson and Merzlyak, 1996)	328.08±7.89^{c}	338.56± 6.09^{bc}	376.56±6.59^{a}	330.00±3.87^{c}	351.40±6.36^{b}
676	methylated anthocyanins (Saha et al., 2020) acylated anthocyanins (Saha et al., 2020) protein-tannins complexes (Aleixandre-Tudo and du Toit, 2018) chlorophyll *a* (Merzylak at al., 2003)	2120.40±2.08^{d}	2380.85±30.04^{b}	2577.83 ±20.70^{a}	2112.63±19.92^{d}	2242.61±18.08^{c}
Sum of peak areas, [R(%)·nm]		4934.61	5413.80	5655.22	4731.82	5029.71

a-d lowercase superscript letters in the same row for each wavelength are significantly different ($p < 0.05$).

to cause intensive polyphenol degradation because its energy was the highest. The highest significant ($p < 0.05$) increases in the peak areas were obtained for the compounds at 404, 456, and 508 nm under white light and at 568, 621, and 676 nm under red-orange light.

Based on the sum of the peak areas of the identified compounds, the decreases that occurred in GSEP can be ordered as follows: yellow-green-cyan light (7.81 %) < white light (9.19 %) < cyan-blue-violet light (9.33 %) < red-orange light (10.66 %). In the case of GSEB, the sums of the peak areas were higher, 9.71 %, 14.60 %, and 1.93 % for exposures to white, red-orange, and yellow-green-cyan light, and lower, 4.11 % for cyan-blue-violet light. The decreases in both GSEP and GSEB spectra caused by the effect of cyan-blue-violet light agree with the results of the chemical and color analyses. The differences between other light exposures could have arisen from the complexity of the optically active compounds.

4. Conclusions

The study provides insights into the encapsulation of red grape seed extract powder in an alginate–whey protein matrix and the protective effect conferred by this matrix when the beads are exposed to white light and its red-orange, yellow-green-cyan, and cyan-blue-violet components. The ionic gelation of alginate, whey protein concentrate, red grape seed extract, and water in the ratio 1:2:1:100 resulted in the beads with the highest encapsulation efficiency, 88.64 %.

Exposing these red grape seed beads to light affected their morphology to different extents. Apart from the sphericity, which did not change, significant shrinkage occurred, suggesting a rearrangement of the structure to a denser packing. The initial fine cracks in the shells of the beads became deeper, more numerous, and more obvious after light exposure. Changes in geometry of beads upon light exposure could influence the preservation of polyphenols in opposite ways. A denser structure inhibited light penetration and contributed to the protection of polyphenols inside the beads. On the other hand, the increase in the cracks number and depth in the shells of the beads promoted light penetration and a larger contact surface with inner polyphenols.

Regarding the total polyphenol and cyanidin-3-*O*-glucoside contents of the red grape seed extract and beads, their concentrations in GSEB were significantly higher than in GSEP at the end of exposure to white light, yellow-green-cyan light, and red-orange light, showing the protective effect of the alginate–whey protein matrix. For flavonoids, the alginate–whey protein matrix was only effective against the exposure to red-orange light, with significantly higher values observed for GSEB compared to GSEP.

The reflectance spectra of the investigated samples were deconvoluted and showed seven and six groups of colored compounds in GSEP and GSEB, respectively, while their ratios changed with different light exposures. The self-associations of anthocyanins and the co-pigmentation of anthocyanins with other co-factors helped explain the color attributed to unexposed and exposed red grape seed extract powder and beads. The reduction in the peak areas assigned to the wavelengths of the colored compounds in the GSEP and GSEB correlated well with the decreasing flavonoid and cyanidin-3-*O*-glucoside profiles after exposure to cyan-blue-violet light, as determined by the chemical analyses. By highlighting the optically active compound groups and providing evidence of co-pigmentation between anthocyanins or other molecules, the reflectance spectra can be used for semi-quantitative analysis of polyphenols.

From an industrial perspective, these findings are important in deciding whether to use red grape seed extract or red grape seed extract beads for food fortification. Such a decision should consider the compounds to be protected, that is, polyphenols, cyanidin-3-*O*-glucoside, or flavonoids, as well as the colors of visible light to which the fortified foods are intended to be exposed. Further investigation will be conducted on foods containing red grape seed extract beads that are exposed to light to understand the *in vitro* and *in vivo* release of polyphenols.

CRediT authorship contribution statement

A. Mihaly Cozmuta: Writing – original draft, Investigation, Conceptualization. **A. Peter:** Investigation. **C. Nicula:** Investigation. **A. Jastreszbska:** Writing – review & editing, Investigation. **M. Jastrzębska:** Methodology, Investigation. **M.A.K. Purbayanto:** Methodology, Investigation. **A. Bunea:** Writing – review & editing, Methodology, Investigation. **F. Bora:** Writing – review & editing, Methodology, Investigation. **A. Uivarasan:** Writing – review & editing, Investigation. **Z. Szakács:** Writing – review & editing, Methodology, Investigation, Conceptualization. **L. Mihaly Cozmuta:** Validation, Software, Methodology, Investigation.

Declaration of competing interest

The authors declare that they have no known competing financial interests or personal relationships that could have appeared to influence the work reported in this paper.

Data availability

Data will be made available on request.

Acknowledgements

The authors are grateful for the technical support of the Technical University of Cluj Napoca, Romania, University of Agricultural Sciences and Veterinary Medicine Cluj-Napoca, Romania and Warsaw University of Technology, Poland.

Appendix A. Supplementary data

Supplementary data to this article can be found online at https://doi.org/10.1016/j.fochx.2024.101758.

References

Aleixandre-Tudo, J. L., & du Toit, W. (2018). Frontiers and new trends in the science of fermented food and beverages. In R. L. Solís-Oviedo, & Á. de la Cruz Pech-Canul (Eds.), *The role of UV-visible spectroscopy for phenolic compounds quantification in winemaking* (pp. 1–21). IntechOpen. https://doi.org/10.5772/intechopen.73404.

Amico, V., Chillemi, R., Mangiafico, S., Spatafora, C., & Tringali, C. (2008). Polyphenol-enriched fractions from Sicilian grape pomace: HPLC-DAD analysis and antioxidant activity. *Bioresource Technology, 99*(13), 5960–5966. https://doi.org/10.1016/j.biortech.2007.10.037

Anouar, E. H., Gierschner, J., & Duroux, & J.-L., Trouillas, P.. (2012). UV/visible spectra of natural polyphenols: A time-dependent density functional theory study. *Food Chemistry, 131*, 79–89. https://doi.org/10.1016/j.foodchem.2011.08.034

Braidot, E., Petrussa, E., Peresson, C., Patui, S., Bertolini, A., Tubaro, F., … Zancani, M. (2014). Low-intensity light cycles improve the quality of lamb's lettuce (Va. lerianella olitoria [L.] Pollich) during storage at low temperature. *Postharvest Biology and Technology, 90*, 15–23. https://doi.org/10.1016/j.postharvbio.2013.12.003

Chan, L. W., Lee, H. Y., & Heng, P. W. S. P. (2006). Mechanisms of external and internal gelation and their impact on the functions of alginate as a coat and delivery system. *Carbohydrate Polymers, 63*(2), 176–187. https://doi.org/10.1016/j.carbpol.2005.07.033

Chi, J., Ge, J., Yue, X., Liang, J., Sun, Y., Gao, X., & Yue, P. (2019). Preparation of nanoliposomal carriers to improve the stability of anthocyanins. *LWT- Food Science and Technology, 109*, 101–107. https://doi.org/10.1016/j.lwt.2019.03.070

Chowdhuri, M., Ngo, V.-D., Islam, M. N., Ali, M., Islam, S., Rasool, K., Park, S.-U., & Chung, S.-O. (2021). Estimation of glucosinolates and anthocyanins in kale leaves grown in a plant factory using spectral reflectance. *Horticulturae, 7*, 56–73. https://doi.org/10.3390/horticulturae7030056

Dabetic, N., Todorovic, V., Malenovic, A., Sobajic, S., & Markovic, B. (2022). Optimization of extraction and hplc–ms/ms profiling of phenolic compounds from red grape seed extracts using conventional and deep eutectic solvents. *Antioxidants, 11*, 1595. https://doi.org/10.3390/antiox11081595

D'Souza, C., Yuk, H.-G., Khoo, G. H., & Zhou, W. (2015). Application of light-emitting diodes in food production, postharvest preservation, and microbiological food safety. *Comprehensive Reviews in Food Science and Food Safety, 14*, 719–740. https://doi.org/10.1111/1541-4337.12155

Foti, M. C. (2007). Antioxidant properties of phenols. *Journal of Pharmacy and Pharmacology, 59*, 1673–1685. https://doi.org/10.1211/jpp.59.12.0010

Galleano, M., Verstraeten, S. V., Oteiza, P. I., & Fraga, C. G. (2010). Antioxidant actions of flavonoids: Thermodynamic and kinetic analysis. *Archives of Biochemistry and Biophysics, 501*(1), 23–30. https://doi.org/10.1016/j.abb.2010.04.005

Giovenzana, V., Civelli, R., Beghi, R., Oberti, R., & Guidetti, R. (2015). Testing of a simplified LED based Vis/NIR system for rapid ripeness evaluation of white grape (Vitis vinifera L.) for Franciacorta wine. *Talanta, 144*(1), 584–591. https://doi.org/10.1016/j.talanta.2015.06.055

Gitelson, A. A., & Merzlyak, M. N. (1996). Signature analysis of leaf reflectance spectra: Algorithm development for remote sensing of chlorophyll. *Journal of Plant Physiology, 148*(3–4), 494–500. https://doi.org/10.1016/S0176-1617(96)80284-7

Gómez-Mejía, Vicente-Zurdo, D., Rosales-Conrado, N., León-González, E. M., & Madrid, Y. (2022). Screening the extraction process of phenolic compounds from pressed grape seed residue: Towards an integrated and sustainable management of viticultural waste. *LWT- Food Science and Technology, 169*(1), 113988. https://doi.org/10.1016/j.lwt.2022.113988

González-Manzano, S., Santos-Buelga, C., Dueñas, M., Rivas-Gonzalo, J. C., & Escribano-Bailón, T. (2008). Colour implications of self-association processes of wine anthocyanins. *European Food Research and Technology, 226*, 483–490. https://doi.org/10.1007/s00217-007-0560-9

Hadi, J., Wu, S., & Brightwell, G. (2020). Antimicrobial blue light versus pathogenic bacteria: Mechanism, application in the food industry, hurdle technologies and potential resistance. *Foods, 9*, 1895. https://doi.org/10.3390/foods9121895

Hinds, L. M., Bhavya, M. L., O'Donnell, C. P., & Tiwari, B. K. (2022). Electromagnetic technologies in food industry. In V. M. Gómez-López, & R. Bhat (Eds.), *Chapter 7. Visible light*. John Wiley & Sons Ltd. https://doi.org/10.1002/9781119759522.ch7.

Ivanova, V., Dörnyei, Á., Márk, L., Vojnoski, B., Stafilov, T., Stefova, M., & Kilár, F. (2010). Polyphenolic content of Vranec wines produced by different vinification conditions. *Food Chemistry, 124*, 316–325. https://doi.org/10.1016/j.foodchem.2010.06.039

Ji, H.-F., & Shen, L. A. (2008). DFT study on deactivation of triplet excited state riboflavin by polyphenols. *International Journal of Molecular Sciences, 9*, 1908–1914. https://doi.org/10.3390/ijms9101908

Kanner, J. (2020). Polyphenols by generating H_2O_2, affect cell redox signaling, inhibit PTPs and activate Nrf2 axis for adaptation and cell surviving: In vitro, in vivo and human health. *Antioxidants, 9*, 797. https://doi.org/10.3390/antiox9090797

Kim, B., Lee, H., Kim, J., Kwon, K., Cha, H., & Kim, J. (2011). An effect of light emitting diode (LED) irradiation treatment on the amplification of functional components of immature strawberry. *Horticulture, Environment, and Biotechnology, 52*, 35–39. https://doi.org/10.1007/s13580-011-0189-2

Kim, S., Jeong, S., Park, W., Nam, K. C., & DU, A., & Lee S.. (2006). Effect of heating condition of grape seeds on antioxidant activity of grape seeds extracts. *Food Chemistry, 97*, 472–479. https://doi.org/10.1016/j.foodchem.2005.05.027

Kosović, M., Topiař, M., Cuřínová, P., & Sajfrtová, M. (2020). Stability testing of resveratrol and viniferin obtained from *Vitis vinifera* L. by various extraction methods considering the industrial viewpoint. *Scientific Reports, 10*, 5564. https://doi.org/10.1038/s41598-020-62603-w

Lee, Y., Ha, J., Oh, J., & Cho, M. (2014). The effect of LED irradiation on the quality of cabbage stored at a low temperature. *Food Science and Biotechnology, 23*, 1087–1093. https://doi.org/10.1007/s10068-014-0149-6

Leong, J.-Y., Lam, W.-H., Ho, K.-W., Voo, W.-P., Lee, M. F.-X., Lim, H.-P., Lim, S.-L., Tey, B.-T., Poncelet, D., & Chan, E. S. (2016). Advances in fabricating spherical alginate hydrogels with controlled particle designs by ionotropic gelation as encapsulation systems. *Particuology, 24*, 44–60. https://doi.org/10.1016/j.partic.2015.09.004

Li, M., Su, J., Yang, H., Feng, L., Wang, M., Xu, G., … Ma, C. (2023). Grape tartaric acid: Chemistry, function, metabolism, and regulation. *Horticulturae, 9*, 1173. https://doi.org/10.3390/horticulturae9111173

Liu, L., Yang, S., Chen, C., Fang, Y., Li, L., & Ban, Z. (2023). High-performance films fabricated by food protein nanofibrils loaded with vanillin: Mechanism, characterization and bacteriostatic effect. *Food Packaging and Shelf Life, 37*, 101080. https://doi.org/10.1016/j.fpsl.2023.101080

Ma, G., Zhang, L., Setiawan, C. K., Yamawaki, K., Asai, T., Nishikawa, F., Maezawa, S., Sato, H., Kanemitsu, N., & Kato, M. (2014). Effect of red and blue LED light irradiation on ascorbate content and expression of genes related to ascorbate metabolism in postharvest broccoli. *Postharvest Biology and Technology, 94*, 97–103. https://doi.org/10.1016/j.postharvbio.2014.03.010

Mahdavi, S. A., Jafari, S. M., Assadpour, E., & Ghorbani, M. (2016). Storage stability of encapsulated barberry's anthocyanin and its application in jelly formulation. *Journal of Food Engineering, 181*, 59–66. https://doi.org/10.1016/j.jfoodeng.2016.03.003

Merzlyak, M. N., Solovchenko, A. E., & Gitelson, A. A. (2003). Reflectance spectral features and non-destructive estimation of chlorophyll, carotenoid and anthocyanin content in apple fruit. *Postharvest Biology and Technology, 27*, 197–211. https://doi.org/10.1016/S0925-5214(02)00066-2

Mrázková, M., Sumczynski, D., & Orsavová, J. (2023). Influence of storage conditions on stability of phenolic compounds and antioxidant activity values in nutraceutical mixtures with edible flowers as new dietary supplements. *Antioxidants, 12*, 962–989. https://doi.org/10.3390/antiox12040962

Mutalik, S. P., Pandey, A., & Mutalik, S. (2020). Nanoarchitectronics: A versatile tool for deciphering nanoparticle interaction with cellular proteins, nucleic acids and phospholipids at biological interfaces. *International Journal of Biological Macromolecules, 151*(2020), 136–158. https://doi.org/10.1016/j.ijbiomac.2020.02.150

Nile, S. H., Kim, D. H., & Keum, Y.-S. (2015). Determination of anthocyanin content and antioxidant capacity of different grape varieties. *Ciência Técnica Vitivinicola, 30*(2), 60–68. https://doi.org/10.1051/ctv/20153002060

Norman, M., Bartczak, P., Zdarta, J., Ehrlich, H., & Jesionowski, T. (2016). Anthocyanin dye conjugated with Hippospongia communis marine demosponge skeleton and its antiradical activity. *Dyes and Pigments, 134*, 541–552. https://doi.org/10.1016/j.dyepig.2016.08.019

Ouyang, Y., Chen, L., Qian, L., Lin, X., Fan, X., Teng, H., & Cao, H. (2020). Fabrication of caseins nanoparticles to improve the stability of cyanidin 3-O-glucoside. *Food Chemistry, 317*, 126418. https://doi.org/10.1016/j.foodchem.2020.126418

Pedrali, D., Barbarito, S., & Lavelli, V. (2020). Encapsulation of grape seed phenolics from winemaking by products in hydrogel microbeads – Impact of food matrix and processing on the inhibitory activity towards α-glucosidase. *LWT - Food Science and Technology, 133*, 109952. https://doi.org/10.1016/j.lwt.2020.109952

Pedrali, D., Scarafoni, A., Giorgi, A., & Lavelli, V. (2023). Binary alginate-whey protein hydrogels for antioxidant encapsulation. *Antioxidants, 12*, 1192. https://doi.org/10.3390/antiox12061192

Peng, X., Ma, J., Cheng, K. W., Jiang, Y., Chen, F., & Wang, M. (2010). The effects of grape seed extract fortification on the antioxidant activity and quality attributes of bread. *Food Chemistry, 119*(1), 49–53. https://doi.org/10.1016/j.foodchem.2009.05.083

Perumalla, A. V. S., & Hettiarachchy, N. S. (2011). Green tea and grape seed extracts — Potential applications in food safety and quality. *Food Research International, 44* (2011), 827–839. https://doi.org/10.1016/j.foodres.2011.01.022

Reddy, G. V., Sen, A. R., Nair, P. N., Reddy, K. S., Reddy, K. K., & Kondaiah, N. (2013). Effects of grape seed extract on the oxidative and microbial stability of restructured mutton slices. *Meat Science, 95*, 288–294. https://doi.org/10.1016/j.meatsci.2013.04.016

Ribas-Agusti, A., Gratacos-Cubarsi, M., Sarraga, C., Guardia, M. D., Garcia-Regueiro, J. A., & Castellari, M. (2014). Stability of phenolic compounds in dry fermented sausages added with cocoa and grape seed extracts. *LWT- Food Science and Technology, 57*, 329–336. https://doi.org/10.1016/j.lwt.2013.12.046

Rózek, A., Achaerandio, I., Gűel, C., López, M. F., & Ferrando, M. (2009). Grape phenolic impregnation by osmotic treatment: Influence of osmotic agent on mass transfer and product characteristics. *Journal of Food Engineering, 94*(1), 59–68. https://doi.org/10.1016/j.jfoodeng.2009.02.030

Saha, S., Singh, J., Paul, A., & Sarkar, R. (2020). Anthocyanin profiling using UV-vis spectroscopy and liquid chromatography mass spectrometry. *Journal of AOAC International, 103*(1), 23–39. https://doi.org/10.5740/jaoacint.19-0201

Sáyago-Ayerdi, S. G., Brenes, A., & Goñi, I. (2009). Effect of grape antioxidant dietary fiber on the lipid oxidation of raw and cooked chicken hamburgers. *LWT- Food Science and Technology, 42*(5), 971–976. https://doi.org/10.1016/j.lwt.2008.12.006

Sheng, K., Zhang, G., Kong, X., Wang, J., Mul, W., & Wang, Y. (2021). Encapsulation and characterisation of grape seed proanthocyanidin extract using sodium alginate and different cellulose derivatives. *International Journal of Food Science and Technology, 56*, 6420–6430. https://doi.org/10.1111/ijfs.15299

Shi, J., Yu, J., Pohorly, J. E., & Kakuda, Y. (2003). Polyphenolics in grape seeds-biochemistry and functionality. *Journal of Medicinal Food, 6*(4), 291–299. https://doi.org/10.1089/109662003772519831

Vichit, W., Saewan, N., & Thitipromote, N. (2012). Stability of freeze dried encapsulated anthocyanins from black glutinous rice extract. In *PACCON 2012 (Pure and Applied Chemistry International Conference 2012)*. Retrieved from file:///D:/users/computer/downloads/2012Paccon-proceeding-StaencapsulatedND.Pdf at 28.07.2024.

Wu, Y., Hana, Y., Taoa, Y., Li, D., Xie, G., Show, P. L., & Lee, S. Y. (2020). In vitro gastrointestinal digestion and fecal fermentation reveal the effect of different encapsulation materials on the release, degradation and modulation of gut microbiota of blueberry anthocyanin extract. *Food Research International, 132*, 109098. https://doi.org/10.1016/j.foodres.2020.109098

Yadav, K., Bajaj, R. K., Mandal, S., & Mann, B. (2019). Encapsulation of grape seed extract phenolics using whey protein concentrate, maltodextrin and gum arabica blends. *Journal of Food Science and Technology*. https://doi.org/10.1007/s13197-019-04070-4

Yeh, N., Yeh, P., Shih, N., Byadgi, O., & Chih Cheng, T. (2014). Applications of light-emitting diodes in researches conducted in aquatic environment. *Renewable and Sustainable Energy Reviews, 32*, 611–618. https://doi.org/10.1016/j.rser.2014.01.047

Zhang, Z., Zhang, R., Zou, L., & McClements, D. J. (2016). Protein encapsulation in alginate hydrogel beads: Effect of pH on microgel stability, protein retention and protein release. *Food Hydrocolloids, 58*, 308–315. https://doi.org/10.1016/j.foodhyd.2016.03.015